



Multi-directional composite laminates: fatigue delamination propagation in mode I—a comparison

Leslie Banks-Sills · Ido Simon · Tomer Chocron

Received: 23 June 2019 / Accepted: 20 August 2019 / Published online: 29 August 2019
© Springer Nature B.V. 2019

Abstract Double cantilever beam (DCB) specimens composed of carbon fiber reinforced polymer laminate composites were tested. Two material systems were investigated. One consisted of plies from a woven prepreg alternating with tows in the $0^\circ/90^\circ$ -directions and the $+45^\circ/-45^\circ$ -directions. The second was fabricated by means of a wet-layup process with the same multi-directions as the prepreg. In addition, for the second material system, a unidirectional (UD) fabric ply was added. The delamination for this laminate was between the UD fabric and the woven ply with tows in the $+45^\circ/-45^\circ$ -directions. Both fracture resistance R -curve and fatigue delamination propagation tests were carried out. It is found that the initiation value of the interface energy release rate is substantially lower for the wet-layup; whereas, their steady state values are quite similar. The fatigue delamination propagation tests were performed at various cyclic R -ratios. The delamination propagation rate da/dN was calculated from the experimental data and plotted using a modified Paris equation with different functions of the mode I energy release rate. As expected, the da/dN curves

depend upon the R -ratio. By using another parameter based on the Hartman–Schijve equation for metals, it is possible to obtain a master-curve for all R -ratios. It is seen that the propagation rate for the prepreg is faster than that of the wet-layup.

Keywords Constant amplitude · Fatigue delamination growth rate · Fiber reinforced composites · Fracture toughness · Resistance curve · R -ratio

1 Introduction

Composite laminates are being used extensively in aerospace, ship building, medical and sport applications. One of the main disadvantages of these materials is their sensitivity to delamination; that is the separation of adjacent plies (Bolotin 1996; Raju and O'Brien 2008). This is particularly observed for multi-directional (MD) laminates in which adjacent plies have fibers in different directions. There has been much work in characterizing the fracture and fatigue delamination propagation behavior of such materials (Gustafson and Hojo 1987; Hojo et al. 1987, 1994; Sela and Ishai 1989; Hashemi et al. 1990; Martin and Murri 1990; Atodaria et al. 1999; Asp et al. 2001; Martin 2003; Tay 2003; Andersons et al. 2004; Matsubara et al. 2006; Shindo et al. 2006; Argüelles et al. 2008; Shivakumar et al. 2006; Peng et al. 2011; Rans et al. 2011; Jones et al. 2012, 2014, 2015, 2016, 2017; Shahverdi et al. 2012; Banks-Sills et al. 2013; Pas-

L. Banks-Sills (✉) · I. Simon · T. Chocron
Dreszer Fracture Mechanics Laboratory, School of
Mechanical Engineering, Tel Aviv University,
6997801 Ramat Aviv, Israel
e-mail: banks@tau.ac.il

I. Simon
e-mail: idosimon@gmail.com

T. Chocron
e-mail: tomerchocron@mail.tau.ac.il

coe et al. 2013, 2015; Bak et al. 2014; Ishbir et al. 2014; Stelzer et al. 2014; Yao et al. 2014, 2015, 2018; Donough et al. 2015; Khan et al. 2015; Olave et al. 2015; Shiino et al. 2016; Brunner et al. 2017; Mujtaba et al. 2017a, b; Simon et al. 2017; Chocron and Banks-Sills 2019)

Double cantilever beam (DCB) specimens composed of carbon fiber reinforced polymer laminate composites were tested. Two material systems were investigated; one was fabricated from a prepreg and the other by means of a wet-layup process. The materials and methods are presented in Sect. 2. Tests were carried out to determine the load-displacement curve for the quasi-static fracture toughness tests, as well as fatigue delamination propagation of each material system (Simon et al. 2017; Chocron and Banks-Sills 2019). These are described in Sect. 3. Finite element analyses were performed to obtain the energy release rate for both test types. A discussion of these results may be found in Sect. 4. The R -curve for each of the material systems was found and compared in Sect. 5. In addition, delamination fatigue propagation rate curves were compared for each system and also presented in Sect. 5. Ideally, for a particular material system in which the mode I fracture resistance curve and the delamination fatigue propagation rate are known, it would be expected that a damage tolerance approach could be applied for this mode. Unfortunately, it has been seen that delaminations in composite laminates have a high propagation rate. Quantitatively, very high slopes are observed in fatigue delamination propagation curves. Nonetheless, examination of various material systems, as presented here for two, may be used to rank their delamination propagation behavior.

2 Materials and methods

A DCB specimen is shown in Fig. 1. Piano-hinges shown in Fig. 1a were used to apply opening displacements for specimens fabricated from the prepreg; load blocks shown in Fig. 1b were used for the wet-layup. It was found that load blocks result in more stable load application than piano hinges and are preferred. The specimen length, width and thickness are l , b and h , respectively. The initial delamination length a_0 was measured from the center of a piano hinge or a load block hole to the delamination front. For each material type, specimens were cut from a plate using a

water jet process. Nominal dimensions for the specimens are $l = 200$ mm, 20 mm $< b < 30$ mm, 3 mm $< h < 5$ mm. The initial delamination length a_0 was generally about 50 mm. Several prepreg specimens tested quasi-statically had initial delaminations of about 25 mm in length.

Two material systems are compared in this investigation. For the first, the DCB specimens were fabricated from 15 plies each of a plain woven prepreg (G0814/913) arranged in a multi-directional (MD) layup. It may be noted that the fibers in the prepreg are carbon T300. The plies alternated with yarn in the $0^\circ/90^\circ$ -directions and $+45^\circ/-45^\circ$ -directions with the delamination between these two ply types as shown in Fig. 2a. The delamination was between the seventh and eighth ply of the laminate. It was formed by a 25.4 μm thick polytetrafluoroethylene (PTFE) film (Simon et al. 2017). For the second material type, the specimens were fabricated from 19 plies with the delamination between a unidirectional fabric and a woven ply with yarn in the $+45^\circ/-45^\circ$ -directions. The remainder of the plies were woven, with yarn alternating between the $0^\circ/90^\circ$ and $+45^\circ/-45^\circ$ -directions. The delamination was between the tenth (UD) and eleventh (woven) plies as shown in Fig. 2b. This laminate was produced by means of a wet-layup. The carbon fibers are T300. In the UD-fabric, there are about 4% glass fibers by volume transverse to the carbon fibers. These are used to hold the carbon fibers together before creating the layup. The epoxy used to form the laminate is Epikote resin L20 with the hardener Epikure 960 (EPR-L20/EPH-960). In each specimen, an artificial delamination was created by a 13 μm thick PTFE film (Chocron and Banks-Sills 2019). The latter is prescribed in ASTM D5528-13 (2013), ISO 15024 (2001) and ASTM D6115-97 (reapproved 2011) standards for unidirectional composites. All tests were carried out in the spirit of these standards. In Sect. 3, the test procedure will be described.

The High Fidelity Generalized Method of Cells (HFGMC) (Aboudi et al. 2012) was used to determine the mechanical and thermal properties of the various plies for each material type. The properties may be found in Simon et al. (2017) and Chocron and Banks-Sills (2019). Using HFGMC, a homogenization process is carried out so that the plies are treated as anisotropic, homogeneous materials. Each delamination is between two dissimilar plies so that it is treated as an interface crack between two dissimilar anisotropic, homogeneous materials. For UD material, the DCB specimen

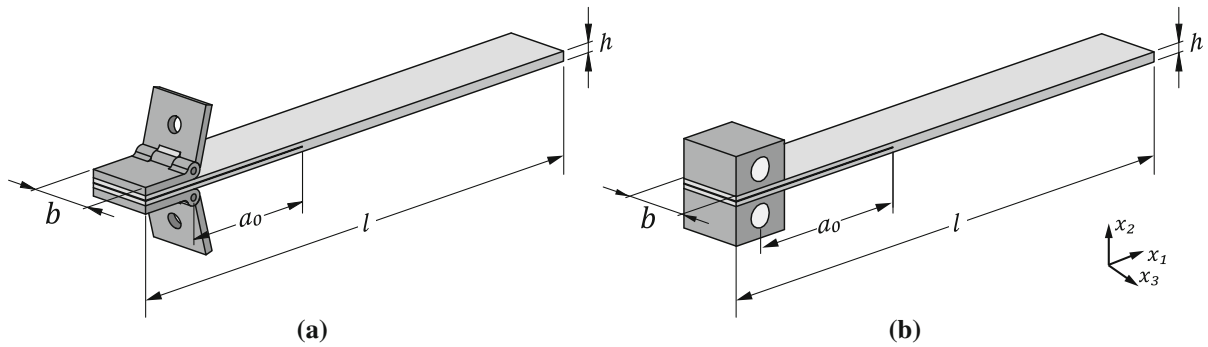


Fig. 1 DCB specimen with **a** piano hinges and **b** load blocks

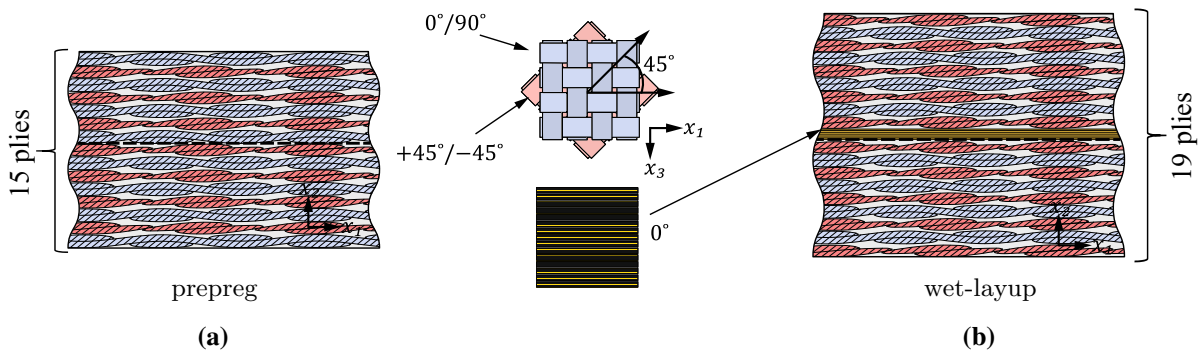


Fig. 2 Schematic view of laminate fabricated **a** from prepreg and **b** by means of a wet-layup. The delamination is along the dashed line

produces pure mode I deformation. Since the delamination here is along an interface, the DCB specimen produces small shear deformation components. These were examined in Simon et al. (2017) and Chocron and Banks-Sills (2019) and seen to be small. Thus, the deformation is nearly that of mode I and the energy release rate is considered as \mathcal{G}_I .

3 Tests

Tests were carried out with an Instron servo-hydraulic loading machine (model number 8872; High Wycombe, UK). The load cell had a maximum capacity of 250 N. For the quasi-static tests, the displacement rate was 1 mm/min in keeping with the standards (ASTM D5528-13 2013; ISO 15024 2001; ASTM D6115-97 reapproved 2011). Quasi-static testing included the fracture toughness tests, as well as the initial part of the fatigue delamination propagation tests. The specimens were stored in an environmental conditioning chamber (M.R.C. BTH80/-20, Holon, Israel) at least one

week before a test was performed with a temperature of $23^\circ \pm 1^\circ \text{C}$ and a relative humidity (RH) of $50 \pm 3\%$. These are within the prescriptions of the ASTM D5528-13 (2013), ISO 15024 (2001) and ASTM D6115-97 (reapproved 2011) standards. The temperature and RH were recorded during the tests.

The fracture toughness tests were carried out on five specimens each for the two material systems. An example of a load versus displacement curve for each material system is illustrated in Fig. 3; other curves are quite similar. For the wet-layup, the initial artificial delamination length a_0 was approximately 54 mm. The approximate value of a_0 for specimens fabricated from the prepreg was 48 mm. It may be observed that the load-displacement curve produced by the wet-layup is stiffer than that for the specimen fabricated from the prepreg. This result appears to be opposite from that expected from the initial delamination length. But the former were thicker, on average (~ 5 mm), than the latter which were about 3.7 mm thick. Indeed, the stiffness does not indicate anything regarding the tough-

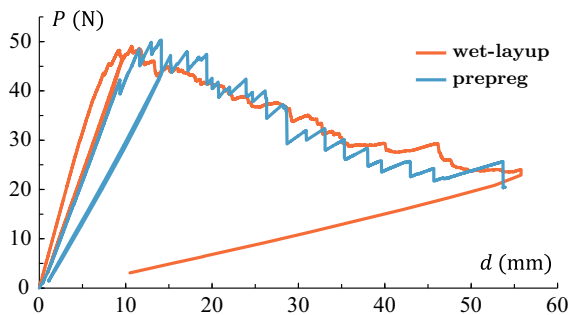


Fig. 3 Load versus displacement curves

ness. After the initial linear response and a short propagation, unloading takes place to a small minimum load. In inducing the precrack from the artificial delamination, the prepreg exhibits a run-arrest behavior. After reloading, the delamination propagates continuously under increasing applied displacement. For the propagating part of the load-displacement curves, values for each specimen type lie within the scatter of the other indicating that the steady state toughness values should be similar. The prepreg propagates in an unstable, run-arrest manner. The wet-layup is almost stable, similar to behavior observed for a UD laminate. Recall that the upper ply of the interface for this material system is a UD fabric. A test protocol was developed and presented in [Simon et al. \(2017\)](#) for the prepreg batch; an update of the protocol was presented in [Chocron and Banks-Sills \(2019\)](#). In both cases, the [ASTM D5528-13 \(2013\)](#), [ISO 15024 \(2001\)](#) and [ASTM D6115-97 \(reapproved 2011\)](#) standards were used as a basis.

The sides of the specimens were painted with white acrylic paint to provide a surface from which to monitor the location of the delamination tip and the delamination length. For the wet-layup, a LaVision digital camera (model Imager Pro SX, Göttingen, Germany) was used to take images of the front side of the specimen edge every 0.5 s. These were automatically synchronized with the load so that the specimens may be analyzed for a given applied load and delamination length to produce the energy release rate versus delamination length. For the prepreg specimens, an older imaging system was used as described in [Simon et al. \(2017\)](#). Discerning the delamination length from the images is difficult and tedious. The analyses are described in [Sect. 4](#).

For the fatigue propagation delamination tests, an initial quasi-static loading was carried out until the

Table 1 Number of specimens tested for each cyclic displacement ratio

	R_d	No. of specimens
Prepreg	0.10	2
	0.33	2
	0.50	2
	0.75	2
Wet-layup	0.10	5
	0.48	4

delamination propagated between 3 and 5 mm. Then, the specimens were subjected to constant amplitude cycles under displacement control. The aim was to carry out 3×10^6 cycles for each test. The test frequency was between 4 and 6 Hz. Thus, the continuous test had a duration generally between 7 and 9 days. The cyclic displacement ratio is defined as

$$R_d = \frac{d_{min}}{d_{max}} \quad (1)$$

where d_{min} and d_{max} are the minimum and maximum actuator displacements in a cycle. For the specimens fabricated from the prepreg, four cyclic displacement ratios were imposed as shown in [Table 1](#) together with the number of specimens tested for each value of R_d . The same information is given for the wet-layup.

As with the fracture toughness tests, the sides of the specimens were painted with white acrylic paint. The delamination tip and length were monitored using the same equipment as that for the fracture toughness tests. From the images and after the test, it was possible to measure the delamination length a as it propagated. Concurrently, values of the load and displacement were also recorded. It may be noted that, here again, there was full synchronization between the load, displacement and images.

In order to obtain a Paris type delamination propagation equation, the delamination length a as a function of the specimen compliance C , as well as a function of the cycle number N are required. Methods for obtaining these relations are presented in [Simon et al. \(2017\)](#) and [Chocron and Banks-Sills \(2019\)](#). The compliance is given by

$$C = \frac{d_{max} - d_{min}}{P_{max} - P_{min}} \quad (2)$$

where the values of the load and displacement are taken from the linear part of the loading cycle. At a number of positions of the delamination length a , the compliance C is calculated from Eq. (2). A curve is fit through these points yielding

$$a = b_1 C^{b_2} \quad (3)$$

Since there is synchronization between the compliance and the cycle number, it is possible to obtain a relation between a and N which is given by

$$a = A_1(N + B_1)^{B_2} + A_2 \quad (4)$$

The non-dimensional constants B_1 and B_2 are determined by means of a nonlinear generalized reduced gradient and the constants A_1 and A_2 by a linear fit; they have dimensions of millimeters. Differentiating Eq. (4) leads to

$$\frac{da}{dN} = A_1 B_2 (N + B_1)^{B_2-1} \quad (5)$$

resulting in a relation between da/dN and N .

4 Finite element analyses

After carrying out the tests, each specimen was analyzed by means of the finite element method to obtain the energy release rate. For both material systems, the energy release rate may be written as

$$\mathcal{G} = \frac{1}{H_1} \left(K_1^2 + K_2^2 \right) + \frac{1}{H_2} K_{III}^2 \quad (6)$$

where H_1 and H_2 are generalized Young's moduli (Simon et al. 2017; Chocron and Banks-Sills 2019), and K_m ($m = 1, 2, III$) are modes 1, 2 and III stress intensity factors. The Arabic numerals are used for the terms representing the square-root, oscillatory singularity and the Roman numerals represent the square-root singularity.

For both material systems, 20 noded, isoparametric brick elements were used in the analyses. For the prepreg (Simon et al. 2017), three-dimensional analyses were carried out, based on the work of Ishbir

et al. (2014), using 83,240 elements. The analyses were carried out using the commercial FE code ADINA (Bathe 2009). The size of elements near the delamination front was about $0.04 \times 0.04 \times 0.4 \text{ mm}^3$. There were 60 elements along the delamination front. The two plies above and below the interface were modeled individually using their effective homogenous, anisotropic material properties given in Table 1 of Simon et al. (2017). The outer plies were modeled as one effective homogenous, anisotropic material with properties also given in Table 1 in Simon et al. (2017). The outer plies are sufficiently far from the interface, so that there is no need to model each ply individually. Contributions of modes 2 and III were found to be negligible. Each contribution was found by means of a conservative interaction energy or M -integral. Hence, the J -integral of ADINA (Bathe 2009) was used to analyze all specimens assuming that

$$\mathcal{G}_I = J. \quad (7)$$

In this way, the total value of the energy release rate was obtained but the mode mixity was neglected and only mode I deformation was assumed. It may be noted that the coefficients of thermal expansion for all plies are identical. Hence, residual curing stresses are minimal and neglected. Only mechanical loading contributes to the value of \mathcal{G}_I .

For the wet-layup (Chocron and Banks-Sills 2019), three-dimensional analyses were also carried out using 310,000 elements. The size of elements near the delamination front was $0.018 \times 0.018 \times 0.5 \text{ mm}^3$. There were 40 elements along the delamination front. The four plies above the interface and the three plies below it were modeled individually using their effective homogenous, anisotropic material properties given in Tables S7 and S9 in Chocron and Banks-Sills (2019). The outer plies were modeled as one effective homogenous, anisotropic material with properties given in Tables S9 and S10 in Chocron and Banks-Sills (2019). Moreover, a mechanical M -integral and a thermal M -integral were used together with the finite element program Abaqus FEA (2017) to analyze the specimens and obtain all mode contributions to the energy release rate. Again here, the contributions of modes 2 and III were small as compared to that of mode 1. Hence, the energy release rate was again referred to as the mode I energy release rate or \mathcal{G}_I and included contributions from all modes.

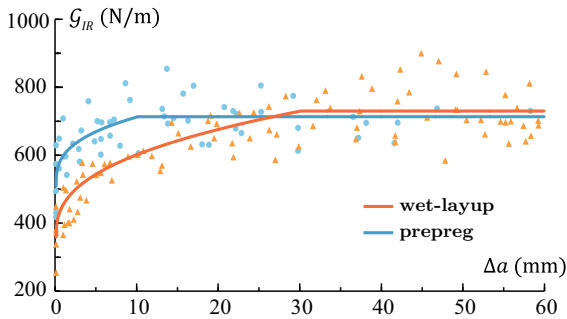


Fig. 4 Fracture resistance curves for prepreg and wet-layup

5 Results

The results obtained for the mode I fracture resistance *R*-curves are presented in Sect. 5.1. In Sect. 5.2, results obtained from the mode I fatigue delamination tests are compared.

5.1 *R*-curve

In this section, the results from the quasi-static, fracture toughness tests are presented. For each specimen, a load vs. displacement curve was obtained two of which are shown in Fig. 3. For the prepreg specimens, the *J*-integral was calculated to obtain a value of G_I given in Eq. (7) for various values of the delamination length. The results are shown in Fig. 4. The value of G_{Ic} at $\Delta a = 0$, where $\Delta a = a - a_0$ (*a* is current delamination length and *a*₀ is the initial delamination length) is 507.5 N/m. The steady state value is $G_{Iss} = 710.5$ N/m which is reached at $\Delta a = 10$ mm. The fitted curve for values $0 < \Delta a < 10$ mm is found as

$$G_{IR} = 93.2\Delta a^{0.339} + 507.5. \tag{8}$$

The coefficient of determination *R*² for this curve is 0.55. For the wet-layup, $G_{Ic} = 357.9$ N/m; $G_{Iss} = 727.7$ N/m for $\Delta a > 30$ mm; and

$$G_{IR} = 100.2\Delta a^{0.384} + 357.9 \tag{9}$$

for $0 < \Delta a < 30$ mm. The coefficient of determination *R*² for this curve is 0.82. It may be observed from Fig. 4 that the wet-layup has a lower value of G_{Ic} than the prepreg. But its steady state value is somewhat higher for this material system.

The *R*-curve of the wet-layup reaches a steady state after a delamination propagation of about 30 mm; while, for the prepreg, a steady state is reached after a propagation of only about 10 mm. This may be related to the amount of propagation required for a steady state process zone to develop near the delamination front. Since the fibers in the prepreg are more constrained by the weave, and fiber bridging is minimal, the process zone is small and steady state is reached earlier than that for the wet-layup. For the latter, the fibers in the UD ply are less constrained and, thus, more fiber bridging may occur as compared to the weave, resulting in a larger process zone which requires a longer propagation to reach steady state.

It is interesting that the steady state behavior of the two laminates is quite similar. Yet the initial fracture toughness values differ significantly. It may be pointed out that initiation G_{Ic} values obtained using Brazilian disk (BD) specimens show a similar ordering for these two material systems (Mega et al. 2019). Moreover, G_{Ic} values obtained using BD specimens were much lower for MD laminates fabricated from UD plies of a different carbon/epoxy material (AS4/3502), with the interface between plies in the 0° and 90°-directions (Banks-Sills et al. 2005), as well as the +45° and -45°-directions (Banks-Sills et al. 2006). Perhaps the UD ply in the wet-layup leads to lower initiation values.

5.2 Fatigue delamination propagation

After the tests were carried out, the specimens were analyzed to determine the value of the energy release rate G_I for each value of *N* from its corresponding values of *a* and the applied load *P*. The Paris type equation may be written as

$$\frac{da}{dN} = D[f(G_I)]^m \tag{10}$$

where *D* and *m* are fitting parameters. Expressions used for *f*(G_I) include G_{Imax} and \hat{G}_{Imax} where

$$\hat{G}_{Imax} = \frac{G_{Imax}}{G_{IR}} \tag{11}$$

G_{Imax} is the maximum value of G_I in a cycle and G_{IR} is the fracture toughness or resistance which depends upon the delamination length. Another function which is used in this work is defined as

Table 2 Energy release rate threshold values

	R_d	R_P	\mathcal{G}_{Ithr} (N/m)
Prepreg	0.10	0.08	30.7
	0.33	0.32	56.1
	0.50	0.48	96.0
	0.75	0.72	331.0
Wet-layup	0.10	0.09	51.5
	0.48	0.45	141.0

$$\Delta\hat{\mathcal{G}}_{Ieff} = \left(\sqrt{\hat{\mathcal{G}}_{Imax}} - \sqrt{\hat{\mathcal{G}}_{Imin}} \right)^2 \tag{12}$$

where $\hat{\mathcal{G}}_{Imax}$ is defined in Eq. (11) and $\hat{\mathcal{G}}_{Imin}$ is defined similarly. The last function considered is

$$f(\mathcal{G}_I) = \Delta\bar{K}_I = \frac{\sqrt{\hat{\mathcal{G}}_{Imax}} - \sqrt{\hat{\mathcal{G}}_{Ithr}}}{\sqrt{1 - \sqrt{\hat{\mathcal{G}}_{Imax}}} } \tag{13}$$

which is based on the Hartman and Schijve (1970) equation for metals. It has been used in various forms in Jones et al. (2012), Brunner et al. (2017), Simon et al. (2017) and Chocron and Banks-Sills (2019). In Eq. (13), $\hat{\mathcal{G}}_{Ithr}$ is the threshold value of $\hat{\mathcal{G}}_{Imax}$. The threshold values for both material systems and cyclic load ratios are found in Simon et al. (2017) and Chocron and Banks-Sills (2019). They are summarized in Table 2 together with the cyclic displacement and load ratios, R_d and R_P , respectively. It may be observed that for the same cyclic displacement ratio R_d , the wet-layup has higher threshold values.

Plotting the fatigue data for both material systems and cyclic displacement ratios using $\hat{\mathcal{G}}_{Imax}$ leads to the schematic representation shown in Fig. 5a. It may be observed that all curves approach the critical energy release rate for high values of da/dN but different threshold values for small values of da/dN . On the other hand, if the fatigue data is plotted using $\Delta\hat{\mathcal{G}}_{Ieff}$, curves such as those shown in Fig. 5b are obtained. In this case, the ordering with respect to the cyclic ratio is reversed and appears in the order that one usually expects for fatigue data in metals. Moreover, for each R -ratio, a different critical value is reached for high values of da/dN ; whereas, one threshold value is reached for all ratios. This fact was used to determine $\hat{\mathcal{G}}_{Ithr}$ (Simon

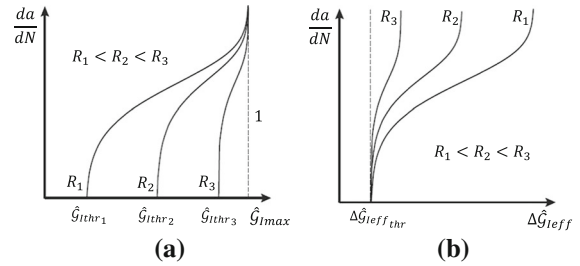


Fig. 5 Schematic description of fatigue test data for different cycle ratios on a log-log scale: da/dN versus **a** $\hat{\mathcal{G}}_{Imax}$ and **b** $\Delta\hat{\mathcal{G}}_{Ieff}$

Table 3 Slopes of Paris type equation for $\hat{\mathcal{G}}_{Imax}$

	R_d	m
Prepreg	0.10	6.8
	0.33	8.0
	0.50	8.9
	0.75	23.0
Wet-layup	0.10	6.1
	0.48	8.8

et al. 2017; Chocron and Banks-Sills 2019). To this end, extrapolation was used to obtain a value of $\Delta\hat{\mathcal{G}}_{Ieff_thr}$. Then, iterations were carried out to determine a master-curve.

Plotting da/dN with respect to either $\hat{\mathcal{G}}_{Imax}$ or $\Delta\hat{\mathcal{G}}_{Ieff}$ leads to very high values of the slope m in Eq. (10). For $\hat{\mathcal{G}}_{Imax}$, these values are presented in Table 3 for each material system and cycle ratio. For the prepreg, each value of m is an average from two tests. For the wet-layup, $m = 6.1$ is the average from five tests and $m = 8.8$ is the average from four tests. For all values of R_d except for $R_d = 0.75$, the slopes are less than 9. As R_d increases, the slope increases as may be observed from the schematic representation in Fig. 5. For $R_d = 0.75$, delamination propagation slows down rapidly as the test progresses causing da/dN to reach small values quickly. This in turn causes the high slope in the da/dN curves. It should be pointed out that the slopes presented here must be multiplied by a factor of two in order to compare them to metals when ΔK_I is being used to plot fatigue propagation rate. For aluminium, $3 < m < 4$. Hence, the delamination propagation rates of laminate composites are much higher than those of metals.

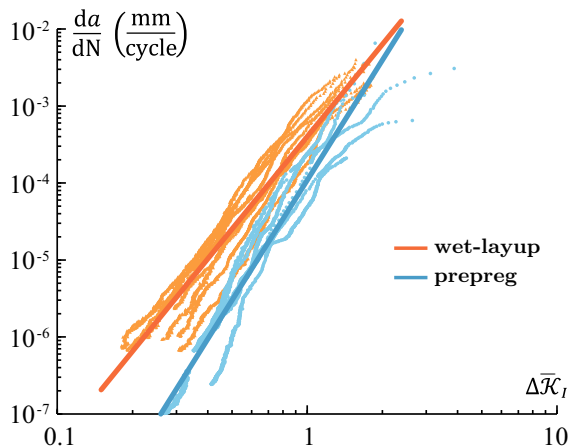


Fig. 6 Delamination propagation rate as a function of $\Delta\bar{K}_I$. Solid lines are master-curves

Table 4 Values of the Paris constants D and m for Eq. (14)

material type	D (mm/cycle)	m
Prepreg	1.10×10^{-4}	5.2
Wet-layup	4.09×10^{-4}	4.0

Using the function in Eq. (13), the results for both material systems are plotted as shown in Fig. 6. The dots are the data from the fatigue delamination propagation tests. The solid lines are the master-curves for each material system given by

$$\frac{da}{dN} = D (\Delta\bar{K}_I)^m \quad (14)$$

where D and m are fitting parameters. Their values for each material system are presented in Table 4. The master-curves provide a full description of fatigue delamination propagation for each material system without dependence on the cycle ratio.

Finally, the fracture surfaces of the specimens subjected to cyclic loading were examined using an Environmental Scanning Electron Microscope (ESEM) (FEI Quanta 200FEG ESEM; Eindhoven, Netherlands). Images of the fracture surfaces of one specimen from each material system are presented in Fig. 7. Both specimens were tested under the same displacement ratio of 0.1. In Fig. 7a, sections of the fracture surfaces with exposed fibers are compared and in Fig. 7b, sections of the fracture surfaces with fiber imprints are presented. There is debris in the latter figure for the wet-

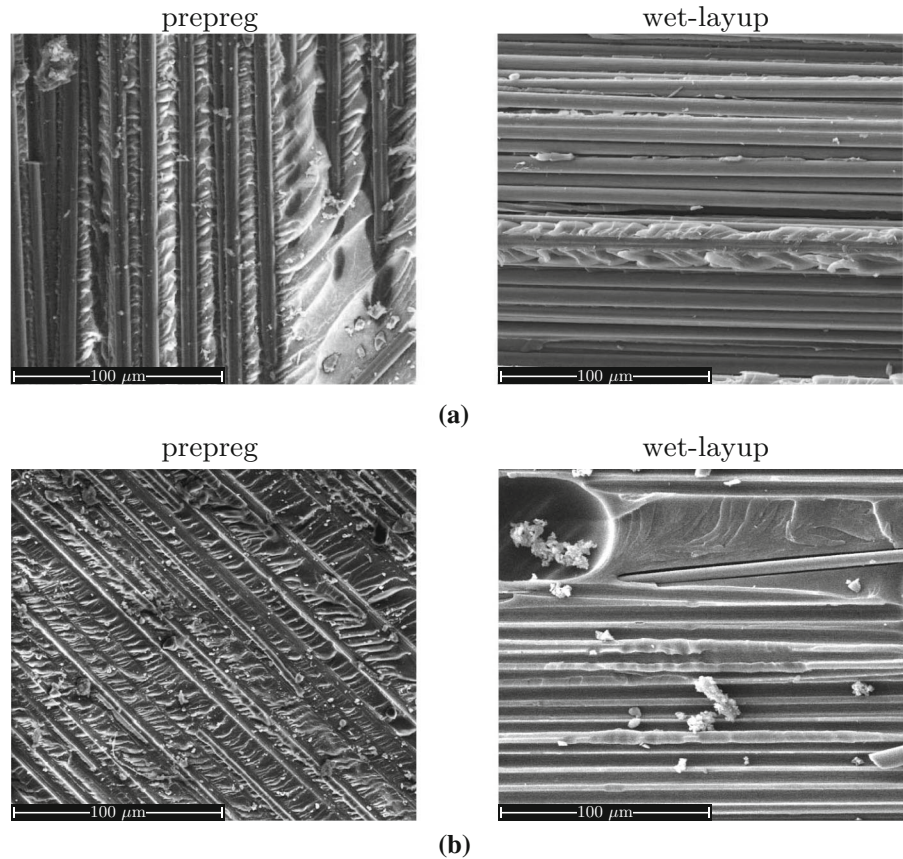
layup caused by sawing the specimen which should be ignored. As may be observed, there is a clear difference between the fracture surfaces of the two material systems. When comparing the images of the exposed fibers shown in Fig. 7a, almost no epoxy matrix is seen in the fractograph of the wet-layup (right); whereas for the prepreg (left), a large amount of epoxy may be observed. Moreover, the exposed epoxy in the prepreg fractograph shows hackle-like markings which were rare in the wet-layup specimens. This difference in the fracture features is clearer when comparing the images showing fiber imprints in Fig. 7b. The fracture surface of the prepreg specimen exhibits many hackle-like markings, while none are observed in the fracture surface of the wet-layup specimen. An additional difference between the two surfaces is the depth of the fiber imprint. Since the fibers are the same in both material systems, thus, having the same fiber diameter, it is clearly seen that the imprints in the prepreg specimen are more shallow than those of the wet-layup. Moreover, the wet-layup material system has a higher porosity than the prepreg; an example of a void may be also observed in Fig. 7b.

Overall, by comparing the fracture surfaces of the two material system, it may be concluded that the prepreg fracture surfaces are richer in features than those of the wet-layup. For the wet-layup, a nearly clean cut is observed between the fibers and epoxy matrix; whereas, for the prepreg, more deformation of the matrix is observed. This may indicate better adhesion between the epoxy matrix and the carbon fibers in the prepreg. Again this supports the previously mentioned findings that the initial fracture toughness is lower for material systems containing UD plies. Furthermore, it is interesting to note, as may be seen in Fig. 6, that the delamination propagation rate da/dN , for the same value of $\Delta\bar{K}_I$, was lower for the prepreg. The difference in the fracture surfaces appear to be reflected in the fatigue propagation rate of the two composites.

6 Conclusions

Nearly mode I fracture toughness and fatigue delamination propagation tests were carried out previously on DCB laminate specimens composed of two different material systems. Carbon fiber reinforced polymer material was used in a prepreg and a wet-layup. The initial fracture toughness of the prepreg was about 30%

Fig. 7 Comparison between the fatigue fracture surfaces, as viewed in ESEM images, of the prepreg and wet-layup material systems: **a** images showing exposed fibers are presented and **b** fiber imprints



higher than that of the wet-layup. The steady state values were quite similar.

The fatigue threshold values of the energy release rate were lower for the prepreg. Perhaps these threshold values may be used in design of structures. The slopes of the da/dN versus $\hat{G}_{I_{max}}$ curves were quite similar for the same cycle ratio. However, they are very high, thus, predicting very high fatigue delamination growth rates. The slope of the Paris type equation for $\Delta\bar{K}_I$ for the wet-layup was lower than that of the prepreg. But the fatigue delamination propagation rate was lower for the latter. The lower values of the slope do not predict moderately propagating delaminations. A small change in applied load leads to a small change in $\hat{G}_{I_{max}}$ but a large change in $\Delta\bar{K}_I$ (Simon et al. 2017). The conclusion here is that only comparative studies between laminates may be made to assess a more reliable one. Using these results to predict delamination propagation appears bleak. Once a delamination appears in a structure, it is predicted to grow very rapidly.

Furthermore, it should be emphasized that not only does the fabrication method influence the obtained results but also the plies on each side of the delamination. Thus, different interfaces require a set of tests such as those described here. It does not appear wise to extrapolate these results to other material systems.

References

- Abaqus FEA (2017) Version 6.17. Dassault Systèmes Simulia Corp., Johnson, RI
- Aboudi J, Arnold SM, Bednarczyk BA (2012) Micromechanics of composite materials: a generalized multiscale analysis approach. Butterworth-Heinemann, Amsterdam
- Andersons J, Hojo M, Ochiai S (2004) Empirical model for stress ratio effect on fatigue delamination growth rate in composite laminates. *Int J Fatigue* 26(6):597–604
- Argüelles A, Viña J, Canteli AF, Castrillo MA, Bonhomme J (2008) Interlaminar crack initiation and growth rate in a carbon-fibre epoxy composite under mode-I fatigue loading. *Compos Sci Technol* 68(12):2325–2331

- Asp LE, Sjögren A, Greenhalgh ES (2001) Delamination growth and thresholds in a carbon/epoxy composite under fatigue loading. *J Compos Tech Res* 23(2):55–68
- ASTM D6115-97 (reapproved 2011) (2011) Standard test method for mode I fatigue delamination growth onset of unidirectional fiber-reinforced polymer matrix composites. In: *Space simulation; aerospace and aircraft; composite materials*, vol 15.03. ASTM International, West Conshohocken
- ASTM D5528-13 (2013) Standard test method for mode I interlaminar fracture toughness of unidirectional fiber-reinforced polymer matrix composites. *Space simulation; aerospace and aircraft; composite materials*, vol 15.03. ASTM International, West Conshohocken
- Atodaria DR, Putatunda SK, Mallick PK (1999) Delamination growth behavior of a fabric reinforced laminated composite under mode I fatigue. *J Eng Mater Technol* 121(3):381–385
- Bak BLV, Sarrado C, Turon A, Costa J (2014) Delamination under fatigue loads in composite laminates: a review on the observed phenomenology and computational methods. *Appl Mech Rev* 66(6):060803
- Banks-Sills L, Boniface V, Eliasi R (2005) Development of a methodology for determination of interface fracture toughness of laminate composites—the $0^\circ/90^\circ$ pair. *Int J Solids Struct* 42(2):663–680
- Banks-Sills L, Freed Y, Eliasi R, Fourman V (2006) Fracture toughness of the $+45^\circ / -45^\circ$ interface of a laminate composite. *Int J Fract* 141(1–2):195–210
- Banks-Sills L, Ishbir C, Fourman V, Rogel L, Eliasi R (2013) Interface fracture toughness of a multi-directional woven composite. *Int J Fract* 182(2):187–207
- Bathe KJ (2009) ADINA-automatic dynamic incremental non-linear analysis, version 8.6.0. ADINA R&D Inc, Watertown
- Bolotin VV (1996) Delaminations in composite structures: its origin, buckling, growth and stability. *Compos Part B-Eng* 27(2):129–145
- Brunner AJ, Stelzer S, Mujtaba A, Jones R (2017) Examining the application of the Hartman-Schijve equation to the analysis of cyclic fatigue fracture of polymer-matrix composites. *Theor Appl Fract Mech* 92:420–425
- Chocron T, Banks-Sills L (2019) Nearly mode I fracture toughness and fatigue delamination propagation in a multidirectional laminate fabricated by a wet-layup. *Phys Mesomech* 22(2):107–140
- Donough MJ, Gunnion AJ, Orifici AC, Wang CH (2015) Scaling parameter for fatigue delamination growth in composites under varying load ratios. *Compos Sci Technol* 120:39–48
- Gustafson CG, Hojo M (1987) Delamination fatigue crack growth in unidirectional graphite/epoxy laminates. *J Reinf Plast Compos* 6(1):36–52
- Hartman A, Schijve J (1970) The effects of environment and load frequency on the crack propagation law for macro fatigue crack growth in aluminium alloys. *Eng Fract Mech* 1(4):615–631
- Hashemi S, Kinloch AJ, Williams JG (1990) The analysis of interlaminar fracture in uniaxial fibre-polymer composites. *Proc R Soc Lond A* 427(1872):173–199
- Hojo M, Tanaka K, Gustafson CG, Hayashi R (1987) Effect of stress ratio on near-threshold propagation of delamination fatigue cracks in unidirectional CFRP. *Compos Sci Technol* 29(4):273–292
- Hojo M, Ochiai S, Gustafson CG, Tanaka K (1994) Effect of matrix resin on delamination fatigue crack growth in CFRP laminates. *Eng Fract Mech* 49(1):35–47
- Ishbir C, Banks-Sills L, Fourman V, Eliasi R (2014) Delamination propagation in a multi-directional woven composite DCB specimen subjected to fatigue loading. *Compos Part B-Eng* 66:180–189
- ISO 15024 (2001) Fiber reinforced plastic composites—determination of mode I interlaminar fracture toughness, G_{Ic} , for unidirectional reinforced materials. ISO, Geneva
- Jones R, Pitt S, Brunner AJ, Hui D (2012) Application of the Hartman-Schijve equation to represent mode I and mode II fatigue delamination growth in composites. *Compos Struct* 94(4):1343–1351
- Jones R, Stelzer S, Brunner AJ (2014) Mode I, II and mixed mode I/II delamination growth in composites. *Compos Struct* 110:317–324
- Jones R, Hu W, Kinloch AJ (2015) A convenient way to represent fatigue crack growth in structural adhesives. *Fatigue Fract Eng Mater Struct* 38(4):379–391
- Jones R, Kinloch AJ, Hu W (2016) Cyclic-fatigue crack growth in composite and adhesively-bonded structures: the FAA slow crack growth approach to certification and the problem of similitude. *Int J Fatigue* 88:10–18
- Jones R, Kinloch AJ, Michopoulos JG, Brunner AJ, Phan N (2017) Delamination growth in polymer-matrix fibre composites and the use of fracture mechanics data for material characterisation and life prediction. *Compos Struct* 180:316–333
- Khan R, Alderliesten RC, Badshah S, Benedictus R (2015) Effect of stress ratio or mean stress on fatigue delamination growth in composites: critical review. *Compos Struct* 124:214–227
- Martin R (2003) Delamination fatigue. In: Harris B (ed) *Fatigue in composites: science and technology of the fatigue response of fibre-reinforced plastics*, chap. 6. Woodhead Publishing Ltd., Cambridge, pp 173–188
- Martin RH, Murri GB (1990) Characterization of mode I and mode II delamination growth and thresholds in AS4/PEEK composites. In: Garbo SP (ed) *Composite materials: testing and design (ninth volume)*, ASTM-STP 1059. ASTM International, Philadelphia, pp 251–270
- Matsubara G, Ono H, Tanaka K (2006) Mode II fatigue crack growth from delamination in unidirectional tape and satin-woven fabric laminates of high strength GFRP. *Int J Fatigue* 28(10):1177–1186
- Mega M, Dolev O, Banks-Sills L (2019) Two and three - dimensional failure criteria for laminate composites. In preparation
- Mujtaba A, Stelzer S, Brunner AJ, Jones R (2017a) Influence of cyclic stress intensity threshold on the scatter seen in cyclic mode I fatigue delamination growth in DCB tests. *Compos Struct* 169:138–143
- Mujtaba A, Stelzer S, Brunner AJ, Jones R (2017b) Thoughts on the scatter seen in cyclic mode I fatigue delamination growth in DCB tests. *Compos Struct* 160:1329–1338
- Olave M, Vara I, Usabiaga H, Aretxabaleta L, Lomov SV, Vandepitte D (2015) Mode I fatigue fracture toughness of woven laminates: nesting effect. *Compos Struct* 133:226–234
- Pascoe JA, Alderliesten RC, Benedictus R (2013) Methods for the prediction of fatigue delamination growth in composites and

- adhesive bonds—a critical review. *Eng Fract Mech* 112:72–96
- Pascoe JA, Alderliesten RC, Benedictus R (2015) On the relationship between disbond growth and the release of strain energy. *Eng Fract Mech* 133:1–13
- Peng L, Zhang J, Zhao L, Bao R, Yang H, Fei B (2011) Mode I delamination growth of multidirectional composite laminates under fatigue loading. *J Compos Mater* 45(10):1077–1090
- Raju IS, O'Brien TK (2008) Fracture mechanics concepts, stress fields, strain energy release rates, delamination initiation and growth criteria. In: Sridharan S (ed) *Delamination behaviour of composites*, chap. 1. Woodhead Publishing Ltd., Cambridge, pp 3–27
- Rans C, Alderliesten RC, Benedictus R (2011) Misinterpreting the results: how similitude can improve our understanding of fatigue delamination growth. *Compos Sci Technol* 71(2):230–238
- Sela N, Ishai O (1989) Interlaminar fracture toughness and toughening of laminated composite materials: a review. *Composites* 20(5):423–435
- Shahverdi M, Vassilopoulos AP, Keller T (2012) Experimental investigation of *R*-ratio effects on fatigue crack growth of adhesively-bonded pultruded GFRP DCB joints under CA loading. *Compos Part A-Appl S* 43(10):1689–1697
- Shiino MY, Alderliesten RC, Donadon MV, Cioffi MOH (2016) A brief discussion on (pure mode I) fatigue crack growth rate data in 5HS weave fabric composites: evaluation of empirical relations. *Int J Fatigue* 84:97–103
- Shindo Y, Inamoto A, Narita F, Horiguchi K (2006) Mode I fatigue delamination growth in GFRP woven laminates at low temperatures. *Eng Fract Mech* 73(14):2080–2090
- Shivakumar K, Chen H, Abali F, Le D, Davis C (2006) A total fatigue life model for mode I delaminated composite laminates. *Int J Fatigue* 28(1):33–42
- Simon I, Banks-Sills L, Fourman V (2017) Mode I delamination propagation and *R*-ratio effects in woven composite DCB specimens for a multi-directional layup. *Int J Fatigue* 96:237–251
- Stelzer S, Brunner AJ, Argüelles A, Murphy N, Cano GM, Pinter G (2014) Mode I delamination fatigue crack growth in unidirectional fiber reinforced composites: results from ESIS TC4 round-robins. *Eng Fract Mech* 116:92–107
- Tay TE (2003) Characterization and analysis of delamination fracture in composites: an overview of developments from 1990 to 2001. *Appl Mech Rev* 56(1):1–32
- Yao L, Alderliesten RC, Zhao M, Benedictus R (2014) Discussion on the use of the strain energy release rate for fatigue delamination characterization. *Compos Part A-Appl S* 66:65–72
- Yao L, Alderliesten RC, Benedictus R (2015) Interpreting the stress ratio effect on delamination growth in composite laminates using the concept of fatigue fracture toughness. *Compos Part A-Appl S* 78:135–142
- Yao L, Sun Y, Guo L, Lyu X, Zhao M, Jia L, Alderliesten RC, Benedictus R (2018) Mode I fatigue delamination growth with fibre bridging in multidirectional composite laminates. *Eng Fract Mech* 189:221–231

Publisher's Note Springer Nature remains neutral with regard to jurisdictional claims in published maps and institutional affiliations.